Kinetic models for pattern formation in animal aggregations

Buono, Pietro-Luciano; Eftimie, Raluca; Kovacic, Mitchell; van Veen, Lennaert

Published in:
Active Particles, Volume 2

DOI:
10.1007/978-3-030-20297-2_2

Publication date:
2019

Document Version
Peer reviewed version

Kinetic Models for Pattern Formation in Animal Aggregations: a Symmetry and Bifurcation Approach

Pietro-Luciano Buono, Raluca Eftimie, Mitchell Kovacic and Lennaert van Veen

Abstract In this study we start by reviewing a class of 1D hyperbolic/kinetic models (with two velocities) used to investigate the collective behaviour of cells, bacteria or animals. We then focus on a restricted class of nonlocal models that incorporate various inter-individual communication mechanisms, and discuss how the symmetries of these models impact the various types of spatially-heterogeneous and spatially-homogeneous equilibria exhibited by these nonlocal models. In particular, we characterise a new type of equilibria that was not discussed before for this class of models, namely a relative equilibria. Then we simulate numerically these models and show a variety of spatio-temporal patterns (including classic equilibria and relative equilibria) exhibited by these models. We conclude by introducing a continuation algorithm (which takes into account the models symmetries) that allows us to track the solutions bifurcating from these different equilibria. Finally, we apply this algorithm to identify a $\mathbf{D}_3$-symmetric steady-state solution.

1 Introduction

Self-organised behaviours in animal communities have attracted the attention of researchers as well as general public for at least two thousand years. One of the ear-

P-L. Buono
University of Ontario Institute of Technology, Oshawa, ONT, Canada, e-mail: luciano.buono@uoit.ca

R. Eftimie
University of Dundee, Dundee, UK e-mail: r.a.eftimie@dundee.ac.uk

M. Kovacic
Simon Fraser University, Burnaby, BC, Canada e-mail: mkovacic@sfu.ca

L. van Veen
University of Ontario Institute of Technology, Oshawa, ONT, Canada, e-mail: lennaert.vanVeen@uoit.ca

liest recordings of self-organised behaviours can be found in Pliny the Elder's book "Natural History" [54], which describes various aspects of collective dynamics in insects (e.g, bees that cluster "as they do, like a bunch of grapes, upon houses or temples"; book XI), birds (e.g., starlings that "fly in troops, as it were, and then to wheel round in a globular mass like a ball"; book X), fish (e.g., dolphins in [54], which "form among themselves a sort of general community"; book IX) and terrestrial animals (e.g., elephants that "always move in herds"; book $VIII$). Thus, people's attention has always been drawn to the aggregation patterns displayed by these animal aggregations, and the transitions between these patterns. However, these aggregation patterns are the result of how animals communicate with each other: how they perceive/sense their neighbours and how they respond to their neighbours' behaviours. Therefore, to understand the biological mechanisms behind the collective movement and aggregation of animals one needs to to take into account also animal communication.

Mathematical models have been used for almost four decades to propose hypotheses (and then test them *in silico*) regarding the most important biological mechanisms that can explain the observed aggregation patterns [2, 36, 46, 45, 19, 23, 3, 15, 28]. While the initial models (and many of the current models) are described by individual based models (which track the position and velocity of every individual in the population) [58, 19, 16, 15, 53], the lack of analytical techniques that can be used to investigate the diverse patterns obtained with these models lead researchers to concentrate more and more on continuum models (which focus on the density of individuals at generic positions in space) [47, 56, 24, 23, 55, 25]. It should also be emphasised that current research pays also significant attention to multi-scale models that connect individual-based approaches to continuum approaches; see [9, 49, 14, 20] and the references therein. Moreover, the majority of these models for animal collective behaviours focus on the investigation of three basic type of social interactions among individuals (i.e., attraction, repulsion and orientation/alignment) and how these interactions lead to various aggregation patterns [25]. Since these social interactions generally act on different spatial ranges (e.g., repulsion acts on very short ranges, while attraction acts on longer ranges), some of these models are nonlocal. We need to emphasise that only few studies and mathematical models take into account how individuals perceive each other, and how these perception/sensing mechanisms influence the social interactions [24, 23, 21, 22, 10].

In this study, we start by reviewing a class of 1D mathematical models of hyperbolic/kinetic type derived in [23] to describe self-organised behaviours in animal communities as a result of different types of animal communication. (Note that these models are also known as discrete-velocity kinetic models, since they can be recovered from Boltzmann-like kinetic models when we consider only two velocities, namely left and right; see [25].) Such models are known to exhibit a large variety of spatio-temporal patterns, ranging from stationary aggregations that can be time-variant or time-invariant, to different types of moving aggregations (e.g., zigzags); see also the patterns in [23, 11, 12, 22]. Many of these patterns have complex dynamical features, which are still not fully understood in terms of invariant sets of phase space. In Section 3.2 we start discussing different spatially-homogeneous

and spatially-heterogeneous equilibria exhibited by these nonlocal models (some of these equilibria not being studied before), and the symmetry properties of these equilibria. In Section 4 we show numerical simulations of different types of spatio-temporal patterns – including different equilibria – and how these patterns are influenced by the domain boundaries. We also present and discuss a new continuation algorithm (which takes into account the symmetries of the models) that can be used to trace the dynamics of the system from known equilibria to more dynamically exotic patterns in the parameter space.

Since generalisations of 1D hyperbolic models to 2D are more realistic but also more complex, their analytic investigation is more difficult. For this reason, we ignore them in this study.

2 Brief review of 1D hyperbolic/kinetic models for collective dynamics in biology

The last 20 years have seen an increase in the use of hyperbolic/kinetic models that can describe various biological phenomena: from self-organised biological aggregations (i.e., aggregations in the absence of a leader or external stimuli; [23]), to chemotactic aggregations (i.e., aggregations in the presence of a chemotactic signal produced by the members of the group; see [33, 35, 27, 48]), migration of organisms based on food distribution [17], predator-prey dynamics [8, 7] or age-structured models [37, 38, 60].

One of the simplest class of 1D hyperbolic/kinetic models with constant speeds (for individuals moving right and left inside a certain domain) and constant turning rates was introduced and discussed extensively in [35, 32, 34]. The general form of this model for right-moving (u^+) and left-moving (u^-) particles/animals, which includes a turning behaviour ($\lambda^\pm$) as well as a birth/death processes ($h^\pm(u^+,u^-)$), is given by

$$\frac{\partial u^+}{\partial t}+\frac{\partial(\gamma u^+)}{\partial x}=f^+(u^+,u^-)=-\lambda^+u^++\lambda^-u^-+\frac{1}{2}h^+(u^+,u^-), \tag{1a}$$

$$\frac{\partial u^-}{\partial t}-\frac{\partial(\gamma u^-)}{\partial x}=f^-(u^+,u^-)=\lambda^+u^+-\lambda^-u^-+\frac{1}{2}h^-(u^+,u^-). \tag{1b}$$

Here, the turning terms $\lambda^\pm$ describe the probability of right-moving individuals (u^+) to turn around and become left-moving (u^-), as well as the probability of left-moving individuals to turn around and become right-moving. Since the change in the movement direction of cells/bacteria/animals is not always constant, but might depend on (local or nonlocal) interactions with other cells/bacteria/animals, Pfistner [47] and Eftimie et al. [24, 23] considered models of type (1) with constant speeds and nonlocal density-dependent turning rates

$$f^+[u^+,u^-]=-\lambda^+[u^+,u^-]u^++\lambda^-[u^+,u^-]u^-,$$

$f^- = -f^+$, and no birth/death dynamics ($h^\pm = 0$). Because of the complex spatial and spatio-temporal dynamics exhibited by these nonlocal models, in Section 3 we will review in more detail the nonlocal models introduced in [24, 23].

Models of type (1) for the movement of cells/bacteria/animals can be easily coupled with reaction-diffusion models for the dynamics of a chemical ($c(x,t)$) that controls the direction of movement of cells/bacteria/animals (chemical which can be produced by the cells/animals themselves) [33, 48]:

$$\frac{\partial c(x,t)}{\partial t} = p(c,u^+,u^-) + D\frac{\partial^2 c(x,t)}{\partial x^2}, \tag{2}$$

where $p(c,u^+,u^-)$ describes the production/degradation of this chemical, and D is its diffusion rate. The chemical can influence the speed of animals/cells (i.e., $\gamma[u^+,u^-,c]$ in (1)), their turning behaviour and even the birth-death dynamics of the population (i.e., $f^\pm[u^+,u^-,c]$ in (1)).

Regarding the 1D hyperbolic predator-prey models, these do not usually consider turning behaviour (i.e., $\lambda^\pm = 0$) [8], as the two populations are independent (however, the 2D kinetic models can incorporate changes in the movement direction of sub-populations in response to prey/predator behaviour; see [25]). In this case, the functions $f^\pm[u^+,u^-]$ incorporate only the predator-prey dynamics between the two populations. Usually, this dynamics is described by Lotka-Volterra-type terms [18], but other terms such a Holling-type functional responses can also be used [8]. Moreover, the interactions between the prey and predator populations can affect the speed of either prey or predator [18], as the animals speed up to avoid or to catch up with the other population. Note here that not all 1D predator-prey models are of the type (1). For example, Barbera et al. [8] derived a hyperbolic model where the hyperbolic equations for the two populations are coupled with transport equations for the dissipative fluxes.

A final type of hyperbolic model that we would like to mention briefly describes age-structured populations. The hyperbolic age-structured models (of the McKendrick-von Foerster type) have the general form [38]

$$\frac{\partial u(a,t)}{\partial t} + \frac{\partial u(a,t)}{\partial a} = -\lambda(a)u(a,t), \tag{3}$$

with $u(t,a)$ representing the density of the population of age a at time t, and $\lambda(a)$ describing the mortality rate. The description of the model is completed with conditions for the initial population $u(0,a) = Q(a)$, $a \geq 0$, and conditions for the newborn population:

$$u(0,t) = \int_\alpha^\beta u(x,t)m(x)dx, \tag{4}$$

with m the maternity function. Therefore, this class of age-structured models investigate the movement of a population through the age-space.

While all these different hyperbolic models can exhibit a large variety of spatial and spatio-temporal patterns ranging from stationary and moving aggregations of animals/cells (e.g., stationary pulses, travelling pulses, breathers, ripples, zigzags;

see [23]) to networks of cells [27], thorough investigations of these patterns are still not the common approach in mathematical biology. For a more in-depth review of pattern formation in hyperbolic models in biology, and the analytical and numerical techniques available to investigate them, see [21, 59]. Existence of reduction methods (e.g., Centre Manifold reduction) for local bifurcations of various types of equations described in this section has been established for parabolic equations [31], for equations such as (1) in [13] and for hyperbolic age-structured models [44].

Next, we focus on a particular class of nonlocal mathematical models for self-organised biological aggregations, for which there are a few preliminary studies on the local bifurcation of patterns near codimension-1 and codimension-2 bifurcation points [11, 12].

3 Nonlocal 1D hyperbolic models for self-organised animal aggregations via communication

Here, we present in more detail a class of 1D nonlocal hyperbolic models derived to describe the formation and movement of various animal, cell and bacterial aggregations as a result of inter-individual communication [24, 23]. The evolution of densities of right-moving (u^+) and left-moving (u^-) individuals, which travel with constant velocity γ and change their movement direction from right to left (with rate λ^+) and from left to right (with rate λ^-) [23] is given by:

$$\partial_t u^+(x,t) + \partial_x(\gamma u^+(x,t)) = -\lambda^+[u^+,u^-]u^+(x,t) + \lambda^-[u^+,u^-]u^-(x,t), \tag{5a}$$

$$\partial_t u^-(x,t) - \partial_x(\gamma u^-(x,t)) = \lambda^+[u^+,u^-]u^+(x,t) - \lambda^-[u^+,u^-]u^-(x,t), \tag{5b}$$

$$u^\pm(x,0) = u_0^\pm(x). \tag{5c}$$

The turning rates are defined as

$$\begin{aligned}\lambda^\pm[u^+,u^-] &= \lambda_1 + \lambda_2 f(y_r^\pm[u^+,u^-] - y_a^\pm[u^+,u^-] + y_{al}^\pm[u^+,u^-]), \\ &= \Big(\lambda_1 + \lambda_2 f(0)\Big) + \lambda_2\Big(f(y_r^\pm - y_a^\pm + y_{al}^\pm) - f(0)\Big).\end{aligned} \tag{6}$$

The terms $\lambda_1 + \lambda_2 f(0)$ and $\lambda_2\big(f(y^\pm) - f(0)\big)$ describe the baseline random turning rate and the bias turning rate, respectively. The function f is a positive function saturating for large values of its argument (to describe the biologically-realistic situation of bounded turning rates). An example of such function is $f(y) = 0.5 + 0.5\tanh(y)$; see [24, 23, 11, 12]. These turning rates are influenced by the social interactions among individuals: attraction towards far-away neighbours ($y_a^\pm$), alignment with neighbours at intermediate distances ($y_{al}^\pm$) and repulsion from individuals at very close distances ($y_r^\pm$). Moreover, these social interactions depend on the perception of neighbours, which communicate via different mechanisms involving visual, sound, tactile or chemical signals. Table 1 shows the social interaction terms $y_{r,al,a}^\pm$ corresponding to four examples of communication mechanisms introduced in [23]. Note

that in [23] the authors considered also a fifth mechanisms (denoted M1), which combined attraction/repulsion forces as described by M2 and alignment forces as described by M4. Since this mechanisms did not bring any new results in terms of pattern formation or model symmetry, it was ignored in more recent studies [11, 12] and thus we ignore it throughout this study too. The parameters $q_{r,a,al}$ are the magnitudes of the repulsive (r), attractive (a) and alignment (al) interactions. The kernels $K_{r,a,al}$ that model long-distance social interactions are given by Gaussian functions

$$K_j(s) = \frac{1}{2\pi m_j^2} e^{-(s-s_j)^2/(2m_j^2)}, \text{ with } j = r,a,al, \text{ and } m_j = s_j/8, \tag{7}$$

with s_j and m_j, $j = r,a,al$, describing the position and the width of the interaction ranges; see also Fig. 1.

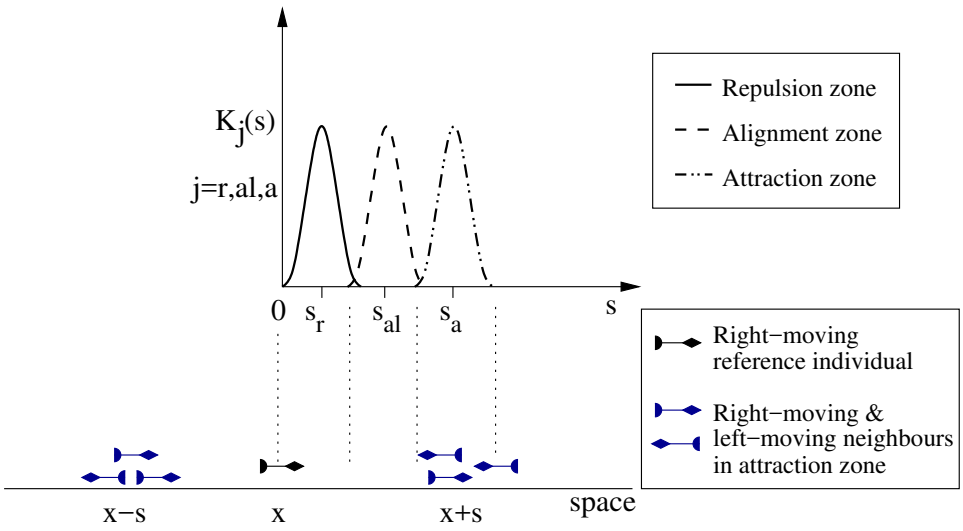

Fig. 1 Kernels K_j, $j = r,al,a$, that model the long-distance social interactions among individuals.

The integrals in Table 1 can be re-written by defining the operator $\mathscr{I}^{\pm}_{i,\ell}(u^+(x),u^-(x),s)$, with $\ell = a,r,al$, to describe the integrand for model Mi, $i = 2,3,4,5$. The superscript $^{\pm}$ in $\mathscr{I}^{\pm}$ corresponds to the superscript in $y^{\pm}$. Thus, the social interaction terms become

$$y^{\pm}_{i,\ell}(u(x)) := \int_0^{\infty} K_\ell(s)\mathscr{I}^{\pm}_{i,\ell}(u^+(x),u^-(x),s)\,ds. \tag{8}$$

Note that $\mathscr{I}^{\pm}$ satisfies the following relation:

$$\mathscr{I}^{\pm}_{i,\ell}(v_1^+(x)+v_2^+(x),v_1^-(x)+v_2^-(x),s) = \mathscr{I}^{\pm}_{i,\ell}(v_1^+(x),v_1^-(x),s)+\mathscr{I}^{\pm}_{i,\ell}(v_2^+(x),v_2^-(x),s),$$

for all $i = 2,3,4,5$ and $\ell = a,r,al$.

Table 1 Nonlocal social interaction terms ($y_j^{\pm}$, $j \in \{a, al, r\}$) introduced in [23]. Constants q_a, q_{al}, q_r describe the magnitudes of the attractive, alignment and repulsive interactions, respectively. Kernels $K_{a,al,r}(s)$ describe the spatial ranges for each of these social interactions. Note that $u = u^+ + u^-$ (total population density).

Mechanisms	Communic. models	Interaction terms: attraction ($y_a^{\pm}$), repulsion ($y_r^{\pm}$), alignment ($y_{al}^{\pm}$)
omnidirectional perception,	M2	$y_{a,r}^{\pm} = q_{r,a}\int_0^{\infty} K_{a,r}(s)\big(u(x\pm s) - u(x\mp s)\big)ds,$
omnidirectional emission		$y_{al}^{\pm} = q_{al}\int_0^{\infty} K_{al}(s)\big(u^{\mp}(x\mp s) + u^{\mp}(x\pm s) - u^{\pm}(x\mp s) - u^{\pm}(x\pm s)\big)ds.$
unidirectional perception,	M3	$y_{r,a}^{\pm} = q_{r,a}\int_0^{\infty} K_{r,a}(s)u(x\pm s)ds,$
omnidirectional emission		$y_{al}^{\pm} = q_{al}\int_0^{\infty} K_{al}(s)\left(u^{\mp}(x\pm s) - u^{\pm}(x\pm s)\right)ds.$
omnidirectional perception,	M4	$y_{r,a}^{\pm} = q_{r,a}\int_0^{\infty} K_{r,a}(s)\left(u^{\mp}(x\pm s) - u^{\pm}(x\mp s)\right)ds,$
unidirectional emission		$y_{al}^{\pm} = q_{al}\int_0^{\infty} K_{al}(s)\left(u^{\mp}(x\pm s) - u^{\pm}(x\mp s)\right)ds.$
unidirectional perception,	M5	$y_{a,r}^{\pm} = q_{r,a}\int_0^{\infty} K_{a,r}(s)u^{\mp}(x\pm s)ds,$
unidirectional emission		$y_{al}^{\pm} = q_{al}\int_0^{\infty} K_{al}(s)u^{\mp}(x\pm s)ds.$

3.1 Boundary conditions

To complete the description of the model (5), and because numerical simulations of system (5) are performed on a finite domain $[0, L]$, we need to describe the boundary conditions. For a detailed discussion of biologically-realistic boundary conditions for hyperbolic systems, see [30, 34]. In the following we discuss in more detail two types of boundary conditions: periodic and reflective.

3.1.1 Periodic boundary conditions

First, we consider periodic boundary conditions, which approximate the dynamics on infinite domains:

$$u^+(0,t) = u^+(L,t), \;\; u^-(L,t) = u^-(0,t). \tag{9}$$

Hillen [34] showed the existence of solutions for *local hyperbolic systems* that satisfy periodic, homogeneous Dirichlet and homogeneous Neumann boundary conditions. Since model (5) is nonlocal, next we confirm that the integrals (8) are well-defined for $u^{\pm}$ satisfying conditions (9). We reproduce the calculation found in [13].

First define the space

$$L^2_{per} = \{u \in L^2(\mathbb{R}) \mid u(x) = u(x+L) \text{ for all } x \in [0,L)\}.$$

We now show that for the interaction kernels $K(s)$ as in (7) and for $v \in L^2_{per}$ and

$$\tilde{K}^{\pm} v(x) := \int_0^{\infty} K(s) v(x \pm s)\, ds, \tag{10}$$

we have $\tilde{K}^{\pm} v(x) \in L^2_{per}$. To this end, we write $v(x) = \sum_{n=-\infty}^{\infty} c_n e^{ik_n x}$, where $k_n = 2\pi n/L$. Then,

$$\begin{aligned}
\tilde{K}^{+} v(x) &= \int_0^{\infty} K(s) \sum_{n=-\infty}^{\infty} c_n e^{ik_n(x+s)}\, ds \\
&= \sum_{n=-\infty}^{\infty} c_n e^{ik_n x} \int_0^{\infty} K(s) e^{ik_n s}\, ds \\
&= \sum_{n=-\infty}^{\infty} c_n \hat{K}(n) e^{ik_n x}.
\end{aligned}$$

Here, $\hat{K}(n)$ is the Fourier transform of $K(s)$, and $\hat{K}(\eta) \to 0$ as $|\eta| \to \infty$ exponentially fast (since $K(s)$ is Gaussian). Next we know that $|c_n|^2 < 1$ if $|n| > N$ for some $N \in \mathbb{N}$:

$$\sum_{n=0}^{\infty} |c_n \hat{K}(n)|^2 \leq \sum_{n=-N}^{N} |c_n|^2 |\hat{K}(n)|^2 + \sum_{n=-\infty}^{-(N+1)} |\hat{K}(n)|^2 + \sum_{n=N+1}^{\infty} |\hat{K}(n)|^2 < \infty.$$

Thus, $\tilde{K}^{+} v(x) \in L^2_{per}$ and the same holds for $\tilde{K}^{-} v(x)$.

Remark 1. Note that if we choose to work with functions in C^0_{per} with the sup-norm $||v||_{\infty} = \sup\{|v(x)| \mid x \in [0,L]\}$, it is a straightforward exercise to show that $\tilde{K}^{\pm}$ is a bounded operator from C^0_{per} to itself.

3.1.2 Reflective boundary conditions

Another type of boundary condition that is commonly used for systems of hyperbolic models (both in biology and physics; see, for example, [39, 40]), is the homogeneous Neumann condition. On the domain $[0, L/2]$, this condition reads

$$u^{+}(0,t) = u^{-}(0,t), \quad u^{+}(L/2,t) = u^{-}(L/2,t), \ t \geq 0. \tag{11}$$

These Neumann (reflective) conditions describe the case where cells/animals cannot leave the domain and turn around at the boundary [43, 30, 34]. In regard to the equivalence between periodic and reflective boundary conditions for local hyperbolic systems, Lutscher [43] and Hillen [34] showed that for solutions that satisfy the mirror symmetry condition

$$u^{+}(x) = u^{-}(L-x), \ x \in [0,L], \tag{12}$$

if one considers $w_0^{\pm}$ the initial data on $[0,L/2]$ that satisfies the no-flux boundary conditions (11), then it can be shown that

$$u_0^{\pm}(x) = \begin{cases} w_0^{\pm}(x) & \text{for } x \in [0,L/2], \\ w_0^{\mp}(L-x) & \text{for } x \in [L/2,L], \end{cases}$$

defines initial data on $[0,L]$ that satisfies periodic boundary conditions. Moreover, considering solutions $u^{\pm}$ of a local version of (5) with periodic boundary conditions (9), one can construct restrictions $w^{\pm}(x,t) = u^{\pm}(x,t)$, for $x \in [0,L/2]$, which are solutions of the same system with no-flux boundary conditions (11).

The steady-state solutions of nonlocal system (5) described below do satisfy the mirror symmetry condition (12). Therefore, the results of the next sections obtained for periodic (or zero-flux) boundary conditions, can be easily generalised to zero-flux (or periodic) conditions.

3.2 Symmetry of hyperbolic models for self-organised biological aggregations

Because the model is built upon a transport term and the interactions between densities at various points, it is not surprising that the model has some symmetry properties. Indeed, as the densities are moving with constant speed, the location in space where the densities are interacting should not matter. This means the model should be translation invariant.

The other symmetry of the model can be understood by thinking of the domain $[0,L)$ as being in between two observers facing each other, but each respecting its own convention. That is, each observer looking at its own left boundary of the interval identifies it as 0. Thus, $[0,L/2)$ for one observer corresponds to $(L/2,L]$ for the facing observer. See Figure 2. Thus, right-moving individuals for one observer at location x are left-moving individuals at location $L-x$ for the other observer. Thus, the spatial reflection $x \mapsto L-x$ is linked to this symmetry. We now formalise these ideas.

We look at functions $u(x,t) = (u^+(x,t), u^-(x,t))$ satisfying the boundary condition $u(0,t) = u(L,t)$. We can define a translation operator T_θ with $\theta \in [0,L)$. With the reflection symmetry on $[0,L)$ defined above, we can also define an involution κ acting on $u(x,t)$:

$$T_\theta \cdot u(x,t) := u(x-\theta,t) \quad \text{and} \quad \kappa \cdot (u^+(x,t), u^-(x,t)) := (u^-(L-x,t), u^+(L-x,t)). \tag{13}$$

Because of the periodic boundary conditions, the domain is a circle and T_θ generates a group isomorphic to $\mathbf{SO}(2)$, the group of rotations on the plane. A direct calculation shows that

$$T_\theta \circ \kappa = \kappa \circ T_\theta^{-1}. \tag{14}$$

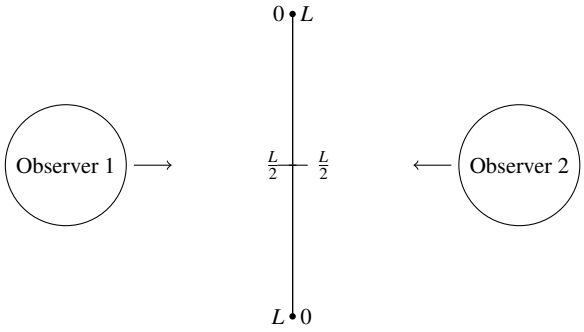

Fig. 2 An interval of length L in between two observers facing each other, where each has its own coordinate convention.

That is, apart from $T_{L/2}$, all rotations do not commute with the involution κ. It is well-known (see [29]) that T_θ and κ along with condition (14) generate a group isomorphic to $\mathbf{O}(2)$, where $\mathbf{O}(2)$ is the orthogonal group and can be thought geometrically as the group of all symmetries of a circle. The operators T_θ and κ are *symmetries* of the model if for any solution $u(x,t)$, then $\kappa \cdot u(x,t)$ and $T_\theta \cdot u(x,t)$ are also solutions for all $\theta \in [0,L)$.

To show formally the symmetry of the model as in [12], one can verify in a straightforward way that the transport portion of the equation is invariant with respect to the translation operator T_θ, where $\theta \in [0,L)$. The turning functions are also symmetric with respect to T_θ because of translation invariance of the integrals. The κ-invariance is derived by verifying that κ acts on the social interaction terms $y_j^{\pm}(x)$ and yields $\kappa \cdot y_j^{\pm}(x) = y_j^{\mp}(L-x)$, and this κ action carries over to the turning functions $\lambda^{\pm}(x)$. Thus, system (5) is $\mathbf{O}(2)$-equivariant for any of the models M2, M3, M4, M5 described in Table 1.

We now define some useful quantities for identifying and classifying the symmetry of solutions. Consider now the action of a group Γ on a function space X. The *isotropy subgroup* of the point $u \in X$ is

$$\Gamma_u := \{\rho \in \Gamma \mid \rho \cdot u = u\}.$$

The symmetry of solutions of (5) is encoded in the isotropy subgroup. To each isotropy subgroup $\Sigma \subset \Gamma$ we define the *fixed-point subspace* of Σ as

$$\mathrm{Fix}(\Sigma) = \{u \in X \mid \sigma \cdot u = u \quad \text{for all } \sigma \in \Sigma\}.$$

Fixed-point subspaces are invariant for the dynamics in Γ-equivariant systems, which can be easily verified by the following calculation. Let $u \in \mathrm{Fix}(\Sigma)$ and let F be Γ-equivariant. Then

$$F(u) = F(\sigma \cdot u) = \sigma \cdot F(u).$$

Let $\Sigma \subset \Gamma$ be a subgroup, then the Σ *group orbit* of an element $u \in X$ is defined as

$$\Sigma u := \{\sigma \cdot u \mid \sigma \in \Sigma\}.$$

In particular, elements lying in the same group orbit have conjugate isotropy subgroups. That is,

$$\Sigma_{\rho \cdot u} = \rho \Sigma_u \rho^{-1}.$$

A *relative equilibrium* is a group orbit invariant for the solution operator of the differential equation; that is, a semiflow-invariant group orbit. In the next section, we present some results about equilibrium (or steady-state) solutions and relative equilibrium solutions.

3.2.1 Equilibria and Relative Equilibria

Equilibrium solutions of (5) are found by setting $\partial_t u^{\pm} = 0$ and solving the remaining integro-differential system. Suppose that $u^*(x) = (u_*^+(x), u_*^-(x))$ is an equilibrium solution with isotropy subgroup Σ. We consider the following two situations for group orbits $\mathbf{O}(2)u^*$ of an equilibrium solution u^*:

1. If $\Sigma = \mathbf{O}(2)$, then $\mathbf{O}(2)u^*$ contains a unique element, and if $\Sigma = \mathbf{SO}(2)$ the group orbit has two elements.
2. If Σ is a discrete subgroup of $\mathbf{O}(2)$, then $\mathbf{O}(2)u^*$ is diffeomorphic to a circle.

In the second situation, we have a circle of equilibrium solutions which is an example of a relative equilibrium, one for which the dynamics is given by the zero vector field on the circle. For a relative equilibrium with a nonzero vector field, one can show that it is a constant vector field which corresponds to the drift generated by the $\mathbf{SO}(2)$ action. It is straightforward to see that adding the two equations in (5) and integrating with respect to x, a steady-state solution $(u_*^+(x), u_*^-(x))$ must then satisfy $u_*^+(x) = u_*^-(x) + C$, where C is a constant. We can now state our new result.

Theorem 1. *Suppose that $\mathbf{O}(2)u^*$ is a relative equilibrium with finite isotropy subgroup Σ.*

1. *If there exists θ such that $\theta\kappa \subset \Sigma$, then $\mathbf{O}(2)u^*$ is a circle of equilibrium solutions and $u^+(x) = u^-(x)$.*
2. *If $\theta\kappa \not\subset \Sigma$ for all $\theta \in \mathbf{SO}(2)$, then generically, the dynamics on $\mathbf{O}(2)u^*$ is given by a $\mathbf{SO}(2)$ drift.*

Before we proceed with the proof, we recall the following facts. The normalizer subgroup of Σ is defined as the largest group in Γ where Σ is normal. In particular, $N(\Sigma) = \{g \in \Gamma \mid g\Sigma g^{-1} \subset \Sigma\}$. The normalizer subgroup is also the largest subgroup in Γ which leaves $\mathrm{Fix}(\Sigma)$ invariant. That is, for any $g \in N(\Sigma)$ and $u \in \mathrm{Fix}(\Sigma)$, then $g \cdot u \in \mathrm{Fix}(\Sigma)$. The normalizer subgroup is also important for determining the flow on a relative equilibrium as we now explain (see for instance Ashwin and Melbourne [4] for all details).

Let x_0 be in the domain of the semiflow generated by solutions of the initially value problem (IVP) and Γx_0 be a relative equilibrium. We denote by $L\Gamma$ the Lie algebra associated with the Lie group Γ. Then $f(x_0) = \zeta x_0$ for some $\zeta \in L\Gamma$. One can refine this result as follows. If x_0 has isotropy subgroup Σ, then $f(x_0) = \zeta x_0$ with $\zeta \in L(N(\Sigma))$; see Proposition 6.1 in [4]. Moreover, generically, the relative equilibrium is foliated by maximal tori in Γ; see Theorem 6.3 in [4]. We can now proceed with the proof of Theorem 1.

Proof. If u^* has isotropy subgroup Σ and $\theta\kappa \subset \Sigma$, then $\Sigma = \mathbf{D}_n$ for some n and $N(\Sigma) = \mathbf{D}_{2n}$. Therefore, $L(N(\Sigma)) = 0$ and so $f(u^*) = 0$. Hence we have a group orbit of equilibrium solutions. In the other case, $\Sigma = \mathbb{Z}_n$ for some n, or $\Sigma = 1$ and $N(\mathbb{Z}_n) = \mathbf{SO}(\mathbf{2})$. The Lie algebra $L(N(\Sigma))$ is isomorphic to $\mathbb{R}$ and by the genericity result stated before this proof we have a maximal torus of dimension one and so $f(x_0) = \zeta x_0$ with ζ nonzero, thus leading to a nonzero drift. □

For homogeneous steady-state solutions, let us first define the total conserved population density

$$A = \frac{1}{L}\int_0^L (u_*^+(x,t) + u_*^-(x,t))\,dx.$$

Then, the homogeneous steady-state solutions are of the form $(u_*^+, u_*^-) = (A/2, A/2)$ and $(u_*^+, u_*^-) = (A^*, A^{**})$, where $A^* \neq A^{**}$ and $A^* + A^{**} = A$. These two types of solutions have isotropy subgroups $\mathbf{O}(\mathbf{2})$ and $\mathbf{SO}(2)$, respectively. We graph these homogeneous steady state solutions in Fig. 3, for u_*^+ versus different model parameters. (Due to model symmetry, similar results can be obtained if we graph $u_*^- = A - u_*^+$ versus model parameters.) We note that all models (M2-M5) described in Table 1 display the steady state with $\mathbf{O}(\mathbf{2})$ symmetry (where $u_*^+ = u_*^-$). In regard to the states with $\mathbf{SO}(2)$ symmetry, the models can exhibit them depending on the parameter values. For example all models M2-M5 can display states with $u_*^+ \neq u_*^-$ when we vary q_{al} and fix all other parameters (as shown in Fig. 3(a)). However, only some models can display such states when we vary A (see models M2 and M4 in panel (b)), λ_1 (see models M2, M3 and M4 in panel (c)) or λ_2 (see models M2 and M4 in panel (d)).

It is also possible to find non-homogeneous symmetric steady-state solutions with isotropy subgroup $\mathbf{D}_n$. Such solutions for $n = 1$ and $n = 3$ are observed in [12, 41].

We now discuss relative equilibria with a nonzero $\mathbf{SO}(\mathbf{2})$ drift. In this case, the isotropy subgroup of the solution is either $\mathbb{Z}_n$ for some $n \geq 2$ or 1. Such solutions can arise for instance from a symmetry-breaking bifurcation from a $\mathbf{D}_n$ or a $\mathbb{Z}_2$ symmetric group orbit of equilibria. The observed pattern is in fact similar to a rotating wave, but as we show below, the speed of rotation must be slow near bifurcation. Meanwhile, for a typical rotating wave arising from an $\mathbf{O}(\mathbf{2})$ symmetric Hopf bifurcation the speed of rotation is arbitrary as it depends on the purely imaginary part of the eigenvalue at bifurcation.

The bifurcations from relative equilibria can be studied by the method described in Krupa [42] for the case of ODEs with compact group symmetry and in Fiedler

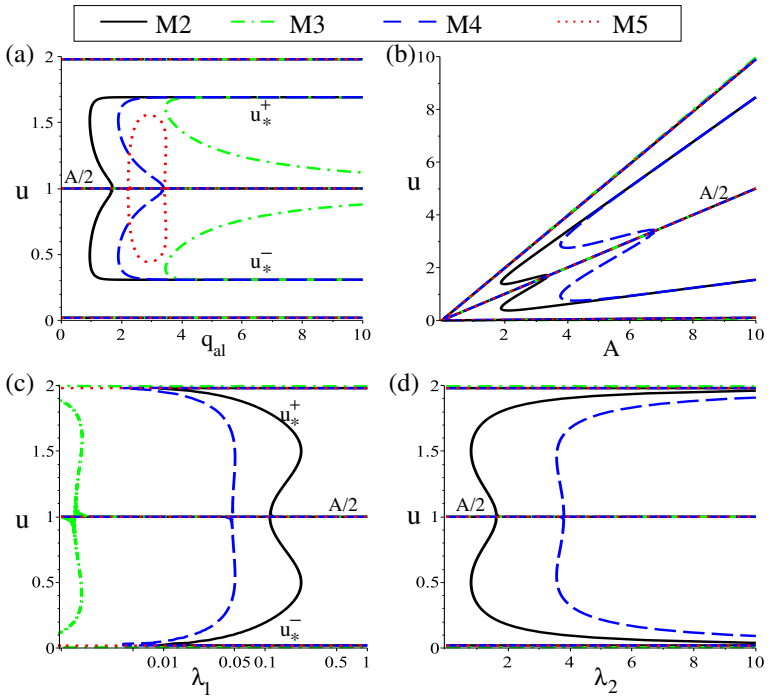

Fig. 3 Spatially homogeneous steady states $u = u_*^+$ displayed by the four models (M2, M3,M4,M5) described in Table 1, as we vary different model parameters: (a) q_{al}; (b) A; (c) λ_1; (d) λ_2. The fixed parameters have the following values: $q_a = 1.0$, $q_r = 0.1$, $q_{al} = 1.0$, $\lambda_1 = 0.2$, $\lambda_2 = 0.9$.

et al [26] for the PDE case, including the case of noncompact groups. Consider a relative equilibrium Γu^* with u^* having isotropy subgroup Σ. The idea is that at each point u_0 of the relative equilibrium, the phase space can be decomposed into the tangent space to the relative equilibrium at u_0, written $T_{u_0}\Gamma u^*$, and a Σ-invariant normal component V contained in the orthogonal complement to $T_{u_0}\Gamma u^*$; see Figure 4.

By this construction, a local centre bundle $\Gamma \times V$ parametrizes a Γ-invariant *tube* in a neighborhood of the relative equilibrium Γu^*. Note that the isotropy subgroup Σ of u^* acts linearly and orthogonally on V. Using these coordinates, the dynamics of the original PDE in the tube is given by

$$\dot{g} = g h_1(v), \qquad \dot{v} = h_2(v),$$

where $(g, v) \in \Gamma \times V$, $L\Gamma$ is again the Lie algebra of Γ, $h_1 : V \to L\Gamma$ and $h_2 : V \to V$. The smoothness of h_1 and h_2 are preserved from the original PDE. According to this representation of the dynamics, relative equilibria in a neighborhood of Γu^* are obtained by solving $h_2(v) = 0$.

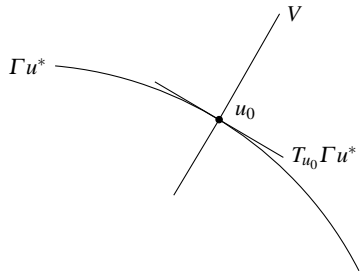

Fig. 4 Decomposition of phase space in the neighborhood of a point u_0 on the relative equilibrium Γu^*.

In the case of an $\mathbf{O}(2)$ group orbit of equilibria given by $\mathbf{O}(2)u^*$, the normal component V is a $\mathbf{D}_n$-invariant codimension-one subspace of phase space. Thus, one obtains the system

$$\dot{g} = gh_1(v), \qquad \dot{v} = h_2(v),$$

where h_1 and h_2 are $\mathbf{D}_n$-symmetric. Because u^* is an equilibrium, we have $h_1(u^*) = h_2(u^*) = 0$.

Consider a one-parameter family of equations (5) parametrized by $\lambda \in \mathbb{R}$ and for which $h_2(u^*, \lambda_0) = 0$. Steady-state bifurcations at the $\mathbf{D}_n$-symmetric equilibrium (u^*, λ_0) follow the generic $\mathbf{D}_n$ symmetric bifurcation theory as described in Golubitsky *et al.* [29]. In particular, steady-state bifurcation problems depend on the parity of n and the kernel of the group action on the eigenspace of the zero eigenvalue of the linearization at the bifurcation point. That is, a steady-state bifurcating from a $\mathbf{D}_n$ equilibrium generically has isotropy subgroup $\mathbf{D}_p$, where p is a divisor of n.

Suppose that for λ near λ_0, $h_2(v^*(\lambda), \lambda) = 0$, then generically $h_1(v^*(\lambda), \lambda) \neq 0$ and in fact must be very close to 0 by continuity. This means that the drift of the relative equilibrium is slow and this is what one should observe in a numerical simulation of a $\mathbf{SO}(2)$ rotating pattern near bifurcation.

4 Numerical results

In this section, we present an overview of model dynamics using a finite-difference based time-stepping scheme, as well as some sample results of the continuation of invariant solutions obtained using a pseudo-spectral scheme. While the former approach is comparatively easy to implement and allows for quick scans of asymptotically stable solutions, the latter has superior convergence properties that are helpful for the accurate approximation of equilibrium and time-periodic solutions, both stable and unstable.

4.1 Model simulations

For the numerical simulations of the dynamics displayed by model (5), we discretise the spatial domain $[0,L]$ into equally-spaced intervals of length Δx, and the time is advanced in steps Δt. The nonlocal terms are discretised using Simpson's method [50]. At the boundaries, the integrals are either wrapped around the domain (for the periodic BCs) or they are reflected back into the domain (for the Neumann BCs). Finally, the advection terms are discretised with the help of the classical upwind/downwind method [50]. Note that we chose Δx and Δt such that the Courant-Friedrichs-Lewy condition is satisfied (i.e., $|\gamma \Delta x/\Delta t| \leq 1$).

Remark 2. We note that while the numerical implementation of the periodic BCs (9) preserves the total population density, the numerical implementation of the reflective BCs (11) for the upwind/downwind method does not preserve this total density. To this end, one needs to slightly change these conditions to:

$$u^+(0,t) = \alpha u^-(0,t), \quad u^-(0,t) = \beta u^+(L,t), \tag{15}$$

with α and β given as follows:

$$\alpha = \frac{\frac{\gamma \Delta x}{\Delta t} + \Delta x \lambda^-[u^+(0,t), u^-(0,t)]}{\frac{\gamma \Delta x}{\Delta t} + \Delta x \lambda^+[u^+(0,t), u^-(0,t)]}, \quad \beta = \frac{\frac{\gamma \Delta x}{\Delta t} + \Delta x \lambda^+[u^+(L,t), u^-(L,t)]}{\frac{\gamma \Delta x}{\Delta t} + \Delta x \lambda^-[u^+(L,t), u^-(L,t)]}, \tag{16}$$

where Δx and Δt are the space and time steps used in the numerical discretisation of the domain.

Finally, the initial conditions for the numerical simulations discussed in the next section are random perturbations of two types of spatially-homogeneous steady states (u_*^+, u_*^-):

- states with $\mathbf{O}(\mathbf{2})$ symmetry: $u_*^+ = u_*^- = A/2 = 1$;
- states with $\mathbf{SO}(2)$ symmetry: $u_*^+ > u_*^-$ or $u_*^+ < u_*^-$ (the exact steady state values depend on model parameters: q_{al}, γ, λ_1, λ_2, as shown in Fig. 3).

The parameters used for the numerical simulations are summarised in Table 2. Any differences from these values are discussed in the figure captions.

4.1.1 Spatio-temporal patterns

We start the presentation of various types of spatio-temporal patterns by focusing on the impact of different boundary conditions. First, we focus on the case where there are a few number of aggregation patterns inside the domain. Figure 5 shows that the patterns localised in the middle of the domain, such as (i) feathers (where individuals leave periodically the aggregations) and (ii) the stationary pulses, are not influenced by the boundary conditions (either (a) periodic or (b) reflective). In contrast, the moving aggregation patterns, such as rotating waves (iii), are affected

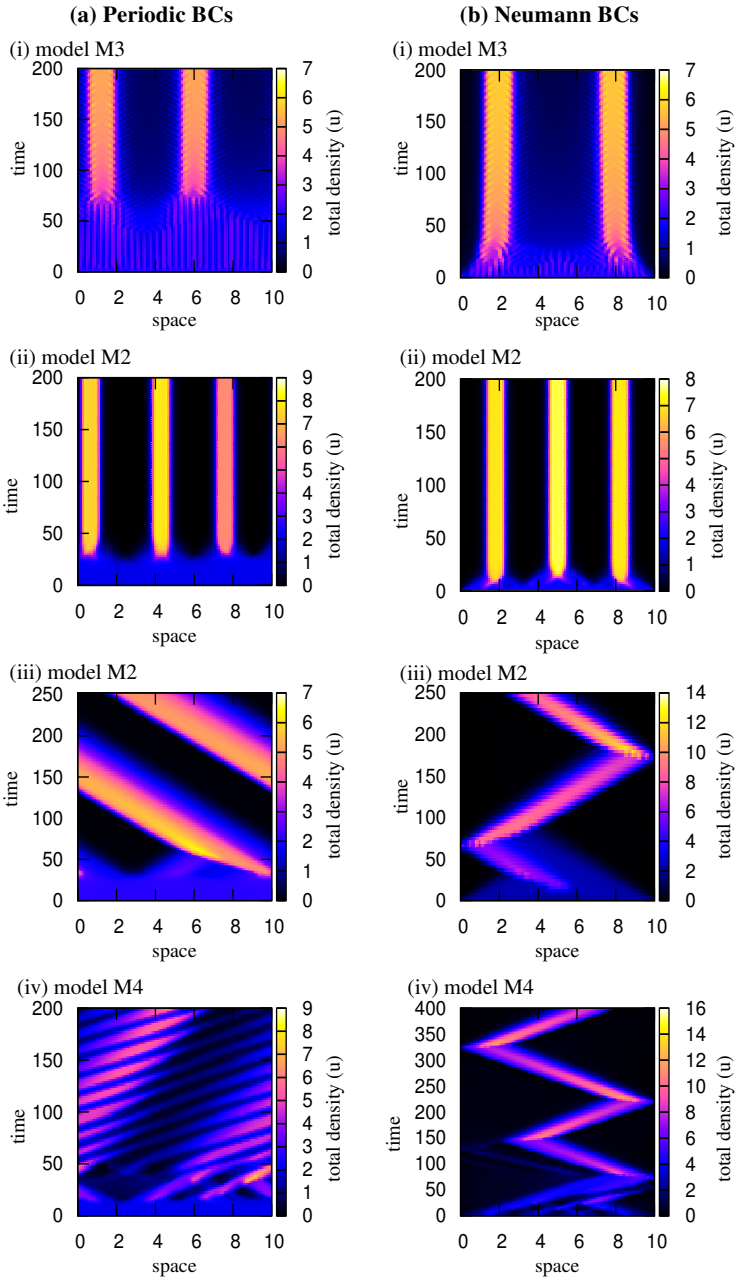

Fig. 5 Examples of stationary and moving aggregation patterns, for different boundary conditions. (a) Periodic boundary conditions (9) on domain $[0,L]$; (b) Neumann (reflective) boundary conditions (15) on domain $[0,L]$. (i) Feather-like patterns obtained with model M3, for $q_{al}=0$, $q_a=6.0$, $q_r=6.4$ [23]; (ii) Stationary pulse patterns obtained with model M2, for $q_{al}=0$, $q_a=4$, $q_r=0.5$; (iii) Travelling pulse (i.e., rotating wave) pattern (left panel), and zigzag pattern (right panel), obtained with model M2, for $q_{al}=2$, $q_a=2$, $q_r=2$; (iv) Modulated travelling pulse (i.e, modulated rotating wave) pattern (left panel), and zigzag pattern (right panel), obtained with model M4 for $q_{al}=2.0$, $q_a=4.0$, $q_r=4.0$.

by the presence of the boundaries. When there are a small number of travelling aggregations inside the domain, these aggregations turn around when they reach the reflective boundary, and move in the opposite direction (thus giving rise to a zigzagging pattern). In contrast, when there are a large number of such travelling aggregations inside the domain, the social interactions between adjacent aggregations and the reflective domain boundaries give rise to stationary aggregations – as shown in Figure 6(d).

Next, we focus on the case when there are multiple aggregations inside the domain. Figure 6 shows a few examples of spatio-temporal patterns obtained when we increase the strength of alignment interactions (while ignoring any repulsive-attractive interactions: $q_a = q_r = 0$). As a transient behaviour we can observe three types of patterns: (a) stationary aggregations, (b) semi-zigzagging aggregations (i.e., stop-and-go waves, where individuals at different positions in space move in one direction, then they stop, only to start moving again in the same direction), (c) travelling aggregations (i.e., rotating waves). Regarding the asymptotic behaviour (observed for $t > 1000$ - not shown here) it is possible to have only stationary aggregations (for $q_{al} = 2.05$ and $q_{al} = 2.18$) and semi-zigzag aggregations (for $q_{al} = 2.15$). Therefore, the semi-zigzag aggregations, which represent a relative equilibrium pattern, are stable and seem to exists in a narrow parameter region.

Next, we investigate numerically the difference between the modulated rotating waves and the semi-zigzag waves. Figure 7 shows on the left the spatio-temporal evolution of the pattern obtained with model M4 (and periodic BCs) when $q_{al} = 2.15$ (and $q_a = 0$, $q_r = 0$, $\lambda_1 = 0.667$, $\lambda_2 = 3.0$ and all other parameter values as in Table 2). For $t < 250$ the model exhibits unstable modulated rotating waves, which then bifurcate for $t > 250$ into stable semi-zigzags (i.e., relative equilibria). The right panels show time snapshots of these two different patterns (for $t = 150$ and $t = 310$). We can see here that both patterns exhibit relatively similar spatial modulations. The difference is that for the semi-zigzags, the high-amplitude solutions (corresponding to the stationary pulses) have a minimum at $u^{\pm}(x,t) \approx 0$ (same as in Fig. 6(a)(ii)), while for the modulated travelling waves the high amplitude solutions have a minimum at $u(x,t) = (u^+ + u^-)(x,t) \gg 0$.

4.2 Continuation algorithm

From Figures 5–7 it seems clear that the various nonlocal models discussed before admit invariant solutions such as equilibria, time-periodic orbits and travelling waves. In order to accurately approximate such solutions, we use a Fourier spectral representation of equations (5a)–(5c). The series expansion is formally given by the Semi Discrete Fourier Transform (SDFT)

$$u^{\pm}(x,t) = \sum_{k=\infty}^{\infty} \hat{u}_k^{\pm}(t) e^{2\pi i k x/L} \; ; \; \hat{u}_k^{\pm}(t) = \frac{1}{L} \int_{x=0}^{L} u^{\pm}(x,t) e^{-2\pi i k x/L} \, \mathrm{d}x. \qquad (17)$$

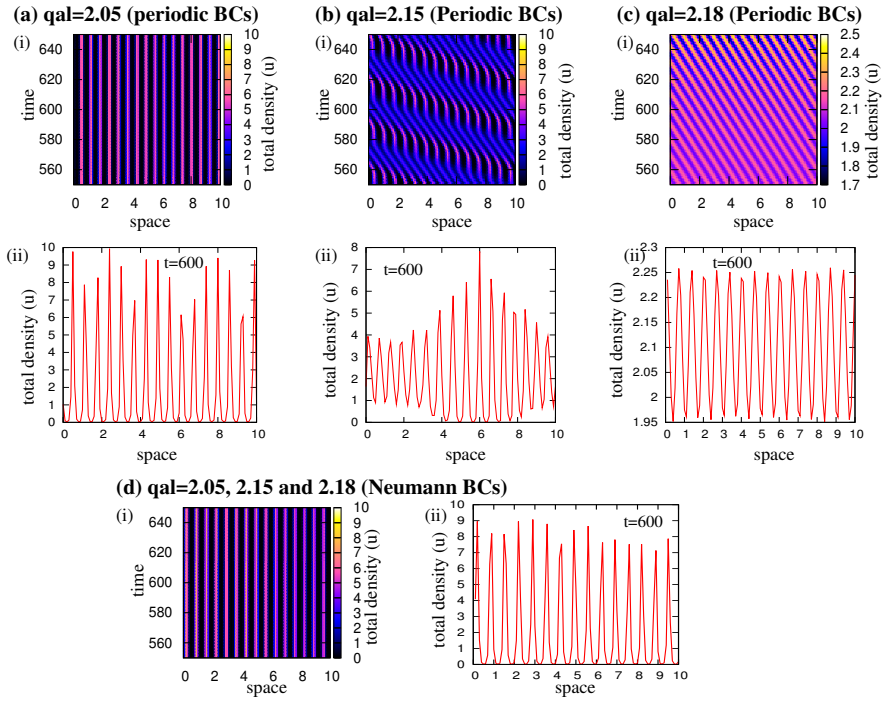

Fig. 6 Example of spatio-temporal patterns obtained with model M4 (see Table 1) for different q_{al} values, while keeping $q_r = q_a = 0.0$. (a) Stationary pulses, obtained for $q_{al} = 2.05$ and periodic BCs; (b) Semi-zigzags obtained for $q_{al} = 2.15$ and periodic BCs; (c) Rotating waves obtained for $q_{al} = 2.18$ and periodic BCs; (d) Stationary pulses obtained for $q_{al} = 2.05$, $q_{al} = 2.15$ and $q_{al} = 2.18$ with Neumann BCs. Sub-panels (i) show the full spatio-temporal pattern, while sub-panels (ii) show Here $\lambda_1 = 0.2/0.3$, $\lambda_2 = 0.9./0.3$. All other parameter values are as described in Table 2

In practice, we retain a finite number of Fourier coefficients, say $|k| \leq M < \infty$. In that case, the above transformation is approximated by the Discrete Fourier Transform (DFT) and a truncation error is introduced. However, it is known that if $u \in C^p[0,L]$ then its Fourier coefficients satisfy $|\hat{u}_k| = \mathrm{O}(k^{-p})$, and if $u \in C^\infty[0,L]$ then $|\hat{u}_k| = \mathrm{O}(\exp[-\alpha k])$ for some $\alpha > 0$ [57]. The truncated Fourier series represents a solution periodic on the domain $[0,L]$, and below we will only consider invariant solutions that satisfy periodic boundary conditions.

The discretised version of equations (5a)–(5c) are obtained by taking the SDFT of the left-hand and right-hand sides. While this is a trivial computation for the linear terms, the nonlinear terms are more involved. We evaluate them in four steps. First, the integral terms are evaluated on the Fourier basis. Since all integrals have the form of convolutions or cross-covariances, they can be evaluated by taking element wise products of the Fourier coefficients of $u^{\pm}$ and the kernels, as done in Section 3.1.1. Secondly, the argument of the nonlinear function f, i.e. $y_r^{\pm} - y_a^{\pm} + y_{al}^{\pm}$, is computed

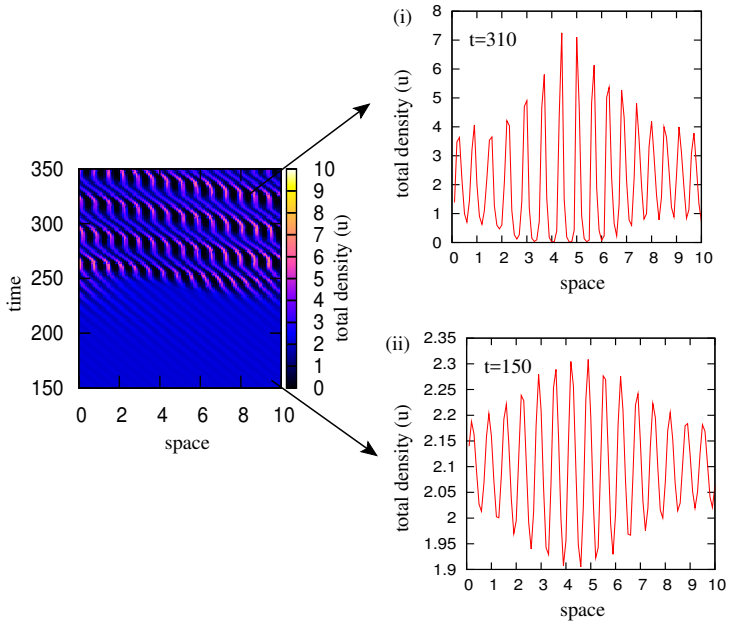

Fig. 7 Transitions between two spatio-temporal patterns obtained with model M4 with periodic BCs, when $q_{al} = 2.15$ (and $q_a = 0$, $q_r = 0$, $\lambda_1 = 0.667$, $\lambda_2 = 3.0$ and all other parameter values as in Table 2). For $t < 250$ we observe modulated rotating waves, while for $t > 250$ we observe semi-zigzags (or relative equilibria). Sub-panels (i) and (ii) show time snapshots of these two different patterns.

on a regular spatial grid using the Fast Fourier Transform algorithm for the inverse DFT. Thirdly, the nonlinear function is evaluated on the grid and, finally, the DFT of the result is computed to find the contribution of the nonlinear terms to the dynamics. This trick of evaluating some terms on the Fourier basis and some on the spatial grid, and using the (inverse) FFT to move from one basis to the other, is often called the pseudo-spectral approach. The most computationally costly step in the process is the FFT, which has an order of complexity of $O(n \ln[n])$, which makes it feasible to evaluate the discretized equations with up to $M = 4096$ modes in less than a second on an average laptop running Matlab, the environment in which our continuation code is written.

The result of this discretisation can be written compactly as

$$\dot{z} = F(z, \lambda), \qquad z(t) = \phi(z(0), t, \lambda), \tag{18}$$

where we have introduce the flow ϕ and the vector Λ of system parameters λ. The vector $z \in \mathbb{R}^{2M}$ holds the real and imaginary parts of the Fourier coefficients of u^+ and u^-. We discretise time by applying the trapezoidal method to the linear terms, and the explicit Euler method to the nonlinear terms. The resulting method is only

first order accurate in time, but since only short integrations are necessary for the computation of invariant solutions this is not a limitation.

Equilibria and periodic solutions relative to the translation symmetry T_θ satisfy

$$\phi(z,P,\Lambda) - T_\theta z = 0. \tag{19}$$

For relative equilibria, P is arbitrary and θ/P is the propagation speed, while for relative periodic solutions P is the period and θ the shift per period. For fixed parameters, each solution to equation (19) that is not spatially homogeneous is embedded in a continuous family because of the translational symmetry in space and, for periodic orbits, in time. If we add phase conditions to remove these degeneracies and vary a single component λ of Λ, we can approximate a curve of solutions using the arclength continuation (see, e.g., [1]). Suppose that we know a solution $(z_\mathrm{p}, P_\mathrm{p}, \lambda_\mathrm{p}, \theta_\mathrm{p})$ and a vector Ξ approximately tangent to the family of solutions, we use Newton iteration so solve

$$\begin{aligned} \phi(z,P,\lambda) - T_\theta z &= 0, \\ \psi(z,P,\lambda,\theta) &= 0, \\ \frac{\mathrm{d}}{\mathrm{d}\theta} T_\theta z_\mathrm{p}\Big|_{\theta=0} \cdot (z - z_\mathrm{p}) &= 0, \end{aligned} \tag{20}$$

$$\Xi \cdot (z - z_\mathrm{p}, P - P_\mathrm{p}, \lambda - \lambda_\mathrm{p}, \theta - \theta_\mathrm{p}) = 0, \tag{21}$$

where, with a slight abuse of notation, we have listed only one system parameter as variable of the flow. The first phase condition is taken to be a Poincaré plane of intersection for periodic orbits, and simply set to $P - c = 0$ for constant c for relative equilibria. Equations (21) constitute a well-posed system of $2M+3$ equations and unknowns. In the implementation we follow [52] and use a Krylov subspace method to approximate the Newton update step. The convergence of Krylov subspace methods depends on the spectrum of the invariant solution under consideration. For equilibrium solutions, we know that this spectrum consists of isolated eigenvalues of finite multiplicity and that there are no accumulation points [13]. The solutions we compute have only a small number of unstable eigenvalues, and thus we expect the spectrum to accumulate in the left half of the complex plane. In practice, we find that the real part of the eigenvalues tends to minus infinity. The corresponding eigenvalues of the linearisation of equation (19), which involves the flow over time P, are thus clustered around minus unity and the Krylov iterations tend to converge rapidly.

Our application of pseudo-spectral discretisation and Newton-Krylov continuation to a dynamical system with spatial interactions described by convolutions is similar to the work of Avitabile *et al.* on a neural mass model [51, 6]. In their model, the convolution represents the integration of synaptic signals originating from a neighbourhood of a given neuron, weighed by the connection density. There is one important difference between the neural field model and the aggregation model. In the former, a sigmoidal functional is applied to the input signal before the convolution is computed. In the aggregation model, we first evaluate the convolution and

then apply the sigmoidal functional. Since applying the functional tends to lead to steep interfaces, while taking the convolution is a smoothing operation, the nonlocal contribution tends to be less smooth in the current model.

It is important to note that, in addition to zero eigenvalues related to exact symmetries of the system, small eigenvalues can exist for certain solutions. For instance, the solution with three pulses shown in Fig. 5(ii) is close to a $\mathbf{D}_3$-invariant solution. Such a solution will generically have a single zero eigenvalue caused by the translational invariance. Numerically, however, we find three eigenvalues close to zero, with eigenvectors corresponding to translations of individual pulses. This is understandable if we consider the fact that the distance between two pulses is about $d = 3$ on a domain of size $L = 10$ (as considered throughout all these numerical simulations). The largest interaction radius is $s_a = 1 = d/3$. Thus, the change to the population density inside each pulse due to the other pulses is small, and the pulses are almost decoupled. Three more small eigenvalues exist that correspond to perturbations that change the height of each of the pulses independently. These small eigenvalues correspond to a near-degeneracy of the linearisation of equations (21), which hampers the convergence of the Newton-Krylov continuation. A practical approach is to restrict the sequence of approximate solutions to lie in the fixed point subspace for the $\mathbf{D}_n$ symmetry. For the three pulse solution, for instance, we can include in z only the Fourier coefficients of wave numbers $k = 3j$, $j \in [\lceil -M/3 \rceil, \lceil M/3 \rceil]$. Thus, we solve a system of equations smaller by a factor of three and exclude the symmetry-breaking, near-zero eigenvalues. This approach was used by Aston *et al.* to compute $\mathbf{D}_n$ symmetric rotating waves [5].

As an example for the application of this algorithm to the identification of new spatially-heterogeneous equilibria, Figure 8 (top) shows a solution (of model M2) approximated by time-stepping for $q_a = 2.4$, $q_{al} = 0$ and $q_r = 0$. Figure 8 (bottom) shows a corrected solution much closer to a $\mathbf{D}_3$ symmetric equilibrium at $q_a = 3.3333$, $q_{al} = 0$ and $q_r = 0.5$. One can see in the power spectrum for the corrected solution that the energy in the high wave numbers do not decay exponentially as they should according to the theory. This is due to the extra eigenvalues near zero described above.

5 Summary and discussion of the results

In this study we reviewed a class of 1D nonlocal hyperbolic models introduced in [23] to describe self-organised animal behaviours, as a result of different types of inter-individual communication. We focused on the symmetry of these models, and discussed some examples of spatio-temporal patterns that can be obtained with two different types of boundary conditions, namely periodic and reflective conditions. In the context of spatially heterogeneous equilibria, we focused on the existence of relative equilibria, and showed in Theorem 1 the conditions for the existence of these equilibria (which have not been previously investigated for this class of 1D nonlocal hyperbolic/kinetic models). This analytical result was complemented by

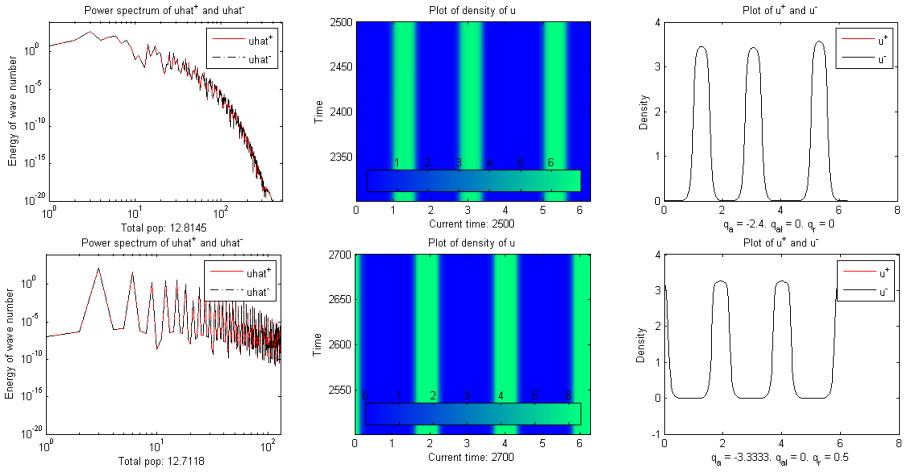

Fig. 8 Top: Power spectrum (left), density plot through time (middle), and final time plot of densities (right) of a solution close to a three bump equilibrium. Bottom: Power spectrum (left), density plot through time (middle), and final time (right) of the corrected solution now showing a three bump equilibrium with the $\mathbf{D}_3$-symmetry more apparent. Note that the q_a value is inserted with a negative sign in the code as one can see below the right pictures.

various numerical simulations showing these types of patterns, and the similarity (in terms of spatial distributions of population density) between relative equilibria patterns and modulated rotating waves.

Finally, we introduced a new continuation algorithm (which considered the symmetry of the solutions) that allowed us to approximate more accurately the equilibria exhibited by this nonlocal class of kinetic models. In Fig. 8 we showed an application of this algorithm to one particular case, the three-pulse solution identified numerically in Fig. 5(ii). We started with the equilibrium solution shown in the top panels in Fig. 8, and we followed it as it developed into another similarly-looking three-bump equilibrium solution, which showed the $\mathbf{D}_3$-symmetry more clearly (i.e., the three peaks in the bottom panel of Fig. 8 all have the same amplitude, while the right peak in the top panel is slightly higher than the other two peaks). While one could apply this algorithm to trace the evolution of known equilibria to more exotic patterns, such an attempt is beyond the scope of this study. Rather, our aim was to briefly describe this algorithm developed for the nonlocal class of kinetic models (5), and to exemplify its applicability to the identification of steady state solutions with $\mathbf{D}_3$-symmetry (while emphasising also the degeneracy of the eigenvalues for the $\mathbf{D}_n$ symmetric solutions).

Acknowledgements PLB and LvV acknowledge the financial support from NSERC in the form of a Discovery Grant.

Appendix

In Table 2 we summarise the parameters that appear in the nonlocal models (5).

Table 2 Summary of model parameters that appear in equations (5) and in Table 1, together with their description and the values used throughout the numerical simulations.

Param.	Value	Description
γ	0.1	Average speed of individuals
λ_1	0.2	Approximation of random turning rate
λ_2	0.9	Approximation of density-directed turning rate
q_r	$0-10$	Strength of repulsive interactions
q_a	$0-10$	Strength of attractive interactions
q_{al}	$0-10$	Strength of alignment interactions
s_r	0.25	Parameter that gives the mid of the repulsion zone
s_{al}	0.5	Parameter that gives the mid of the alignment zone
s_a	1.0	Parameter that gives the mid of the attraction zone
m_r	$s_r/8$	Parameter that controls the width of the repulsion zone
m_{al}	$s_{al}/8$	Parameter that controls the width of the alignment zone
m_a	$s_a/8$	Parameter that controls the width of the attraction zone
L	10	Domain length

References

1. E. L. Allgower and K. Georg. *Introduction to Numerical Continuation Methods*. SIAM, 2003.
2. I. Aoki. A simulation study on the schooling mechanism in fish. *Bull. Jpn. Soc. Sci. Fish*, pages 1081–1088, 1982.
3. S. Arganda, A. Pérez-Escudero, and G.G. de Polavieja. A common rule for decision making in animal collectives across species. *Proc. Matl. Acad. Sci.*, 109:20508–20513, 2012.
4. P. Ashwin and I. Melbourne. Noncompact drift for relative equilibria and relative periodic orbits. *Nonlinearity*, 10:595, 1997.
5. P. J. Aston, A. Spence, and W. Wu. Bifurcation to rotating waves in equations with $o(2)$–symmetry. *SIAM J. Appl. Math.*, 52:792–809, 1992.
6. D. Avitable and K.C.A. Wedgwood. Macroscopic coherent structures in a stochastic neural network: from interface dynamics to coarse-grained bifurcation analysis. *J. Math. Biol.*, 75(4):885–928, 2017.
7. E. Barbera, G. Consolo, and G. Valenti. A two or three compartments hyperbolic reaction-diffusion model for the aquatic food chain. *Math. Biosci. Eng.*, 12(3):451–472, 2015.
8. E. Barbera, C. Currò, and G. Valenti. Wave features of a hyperbolic prey-predator model. *Math. Methods Appl. Sci.*, 33(12):1504–1515, 2010.
9. N. Bellomo, A. Bellouquid, and M. Delitala. From the mathematical kinetic theory of active particles to multiscale modelling of complex biological systems. *Math. Comput. Model.*, 47(7-8):687–698, 2008.
10. A. Berdhal, C.J. Torney, C.C. Ioannou, J.J. Faria, and I.D. Couzin. Emergent sensing of complex environments by mobile animal groups. *Science*, 339(6119):574–576, 2013.

11. P-L. Buono and R. Eftimie. Analysis of Hopf/Hopf bifurcations in nonlocal hyperbolic models for self-organised aggregations. *Math. Models Methods Appl. Sci.*, 24(2):327–357, 2014.
12. P-L. Buono and R. Eftimie. Codimension-two bifurcations in animal aggregation models with symmetry. *SIAM J. Appl. Dyn. Syst.*, 13(4):1542–1582, 2014.
13. P-L. Buono and R. Eftimie. *Lyapunov-Schmidt and Centre Manifold Reduction Methods for Nonlocal PDEs Modelling Animal Aggregations*, volume 157, pages 29–59. Springer Proceedings in Mathematics & Statistics, 2016.
14. D. Burini, L. Gibelli, and N. Outada. A kinetic theory approach to the modeling of complex living systems. In N. Bellomo, P. Degond, and E. Tadmor, editors, *Active Particles*, volume 1, pages 229–258. Birkhäuser, Basel, 2017.
15. D.S. Calovi, U. Lopez, S. Ngo, C. Sire, H. Chaté, and G. Theraulaz. Swarming, schooling, milling: phase diagram of data-driven fish school model. *New Journal of Physics*, 16:015026, 2014.
16. H. Chaté, F. Ginelli, G. Grégoire, F. Peruani, and F. Raynaud. Modeling collective motion: variations on the Vicsek model. *The European Physics Journal B*, 64(3-4):451–456, 2008.
17. S.-H. Choi and Y.-J. Kim. A discrete velocity kinetic model with food metric: chemotaxis travelling waves. *Bull. Math. Biol.*, 79(2):277–302, 2017.
18. R.M. Colombo and E. Rossi. Hyperbolic predators vs. parabolic prey. *Communications in Mathematical Sciences*, 13(2):369–400, 2015.
19. I.D. Couzin, J. Krause, R. James, G.D. Ruxton, and N.R. Franks. Collective memory and spatial sorting in animal groups. *J. Theor. Biol.*, 218:1–11, 2002.
20. P. Degond, A. Frouvelle, S. Merino-Aceituno, and A. Trescases. Quaternions in collective dynamics. *Multiscale Model. Simul.*, 16(1):28–77, 2018.
21. R. Eftimie. Hyperbolic and kinetic models for self-organised biological aggregations and movement: a brief review. *J. Math. Biol.*, 65(1):35–75, 2012.
22. R. Eftimie. Simultaneous use of different communication mechanisms leads to spatial sorting and unexpected collective behaviours in animal groups. *J. Theor. Biol.*, 337:42–53, 2013.
23. R. Eftimie, G. de Vries, and M.A. Lewis. Complex spatial group patterns result from different animal communication mechanisms. *Proc. Natl. Acad. Sci.*, 104(17):6974–6979, 2007.
24. R. Eftimie, G. de Vries, M.A. Lewis, and F. Lutscher. Modeling group formation and activity patterns in self-organizing collectives of individuals. *Bull. Math. Biol.*, 69(5):1537–1566, 2007.
25. R. Fetecau. Collective behaviour of biological aggregations in two dimensions: a nonlocal kinetic model. *Math. Models Methods Appl. Sci.*, 21:1539–1569, 2011.
26. B. Fiedler, S. Björn, A. Scheel, and C. Wulff. Bifurcation form relative equilibria of nonimpact group actions: Skew products, meanders, and drifts. *Documenta Mathematica*, 1:479–505, 1996.
27. F. Filbet, P. Laurencot, and B. Perthame. Derivation of hyperbolic models for chemosensitive movement. *J. Math. Biol.*, 50(2):189–207, 2005.
28. A. Filella, F. Nadal, C. Sire, E. Kanso, and C. Eloy. Model of collective fish behavior with hydrodynamic interactions. *Phys. Rev. Lett.*, 120:198101, 2018.
29. M. Golubitsky, I. Stewart, and D.G. Schaeffer. *Singularities and Groups in Bifurcation Theory. Volume 2*. Springer-Verlag New York Inc., 1988.
30. K.P. Hadeler. Reaction transport equations in biological modeling. *Mathematical and Computer Modelling*, 31(4-5):75 – 81, 2000. Proceedings of the Conference on Dynamical Systems in Biology and Medicine.
31. M. Haragus and G. Iooss. *Local bifurcations, centre manifolds, and normal forms in infinite-dimensional systems*. Springer, 2010.
32. T. Hillen. Invariance principles for hyperbolic random walk systems. *J. Math. Anal. Appl.*, 210(1):360–374, 1997.
33. T. Hillen. Hyperbolic models for chemosensitive movement. *Mathematical Models and Methods in Applied Sciences*, 12(07):1007–1034, 2002.
34. T. Hillen. Existence theory for correlated random walks on bounded domains. *Canad. Appl. Math. Quart*, 18(1):1–40, 2010.

35. T. Hillen and K.P. Hadeler. Hyperbolic systems and transport equations in mathematical biology. In Gerald Warnecke, editor, *Analysis and Numerics for Conservation Laws*, pages 257–279. Springer Berlin Heidelberg, 2005.
36. A. Huth and C. Wissel. The simulation of fish schools in comparison with experimental data. *Ecol. Model*, 75/76:135–145, 1994.
37. H. Inaba. Threshold and stability results for an age-structured epidemic model. *J. Math. Biol.*, 28:411–434, 1990.
38. B.L. Keyfitz and N. Keyfitz. The McKendrick partial differential equation and its uses in epidemiology and population study. *Math. Comput. Modelling*, 26(6):1–9, 1997.
39. I. Kmit. Fredholm solvability of a periodic Neumann problem for a linear telegraph equation. *Ukrainian Mathematical Journal*, 65(3), 2013.
40. I. Kmit and L. Recke. Hopf bifurcation for semilinear dissipative hyperbolic systems. *J. Differerential Equations*, 257:264–309, 2014.
41. M. Kovacic. On matrix-free pseudo-arclength continuation methods applied to a nonlocal pde in 1+1d with pseudo-spectral time-stepping. Master's thesis, University of Ontario Institute of Technology, 2013.
42. M. Krupa. Bifurcations of relative equilibria. *SIAM J. Math. Anal.*, 21(6):1453–1486, 1990.
43. F. Lutscher. Modeling alignment and movement of animals and cells. *J. Math. Biol.*, 45:234–260, 2002.
44. P. Magal and S. Ruan. On integrated semigroups and age structured models in L^p spaces. *Differential Integral Equations*, 20(2):197–239, 2007.
45. J.K. Parrish and L. Edelstein-Keshet. Complexity, pattern, and evolutionary trade-offs in animal aggregations. *Science*, 284(2):99–101, 1999.
46. J.K. Parrish, S.V. Viscido, and D. Grünbaum. Self-organised fish schools: an examination of emergent properties. *Biol. Bull.*, 202:296–305, 2002.
47. B. Pfistner. A one dimensional model for the swarming behaviour of Myxobacteria. In G. Hoffmann W. Alt, editor, *Biological Motion. Lecture Notes on Biomathematics*, pages 556–563. Springer, Berlin, 1990.
48. M. Pineda, C.J. Weijer, and R. Eftimie. Modelling cell movement, cell differentiation, cell sorting and proportion regulation in Dictyostelium discoideum aggregations. *J. Theor. Biol.*, 370:135–150, 2015.
49. W. Pönisch, C.A. Weber, G. Juckeland, N. Biais, and V. Zaburdaev. Multiscale modeling of bacterial colonies: how pili mediate the dynamics of single cells and cellular aggregates. *New Journal of Physics*, 19:015003, 2017.
50. W.H. Press, S.A. Teukolsky, W.T. Vetterling, and B.P. Flannery. *Numerical Recipes: The Art of Scientific Computing*. Cambridge University Press, 2007.
51. J. Rankin, D. Avitabile, J. Baladron, G. Faye, and D. J. B. Lloyd. Continuation of localized coherent structures in nonlocal neural field equations. *SIAM J. Sci. Comp.*, 36:B70–B93, 2014.
52. J. Sánchez Umbría and M. Net. Numerical continuation methods for large–scale dissipative dynamical systems. *Eur. Phys. J. – Spec. Top.*, 225:2465–2486, 2016.
53. A.P. Solon, H. Chaté, and J. Tailleur. From phase to microphase separation in flocking models: the essential role of nonequilibrium fluctuations. *Phys. Rev. Lett.*, 114(6):068101, 2015.
54. Pliny the Elder. *The Natural History*. H.G. Bohn, London, 1855. (Translated by John Bostock M.D. and F.R.S. Henry T. Riley Esq.).
55. C.M. Topaz and A.L. Bertozzi. Swarming patterns in a two-dimensional kinematic model for biological groups. *SIAM J. Appl. Math*, 65(1):152–174, 2004.
56. C.M. Topaz, A.L. Bertozzi, and M.A. Lewis. A nonlocal continuum model for biological aggregation. *Bull. Math. Biol.*, 68:1601–1623, 2006.
57. L. N. Trefethen. *Spectral methods in MATLAB*. SIAM, 2000.
58. T. Vicsek, A. Czirók, E. Ben-Jacob, I. Cohen, and O. Shochet. Novel type of phase transition in a system of self-driven particles. *Phys. Rev. Lett.*, 75:1226, 1995.
59. M. Witten, editor. *Hyperbolic Partial Differential Equations. Populations, reactors, tides and waves: theory and applications*. Pergamon, 1983.
60. D.J. Wollkind. Applications of linear hyperbolic partial equations: predator-prey systems and gravitational instability of nebulae. *Mathematical Modelling*, 7:413–428, 1986.